# Wavelet-Adaptive Interference Cancellation for Underdetermined Platforms: Enhancing Boomless Magnetic Field Measurements on Compact Spacecraft

**ALEX P. HOFFMANN**
**MARK B. MOLDWIN**
University of Michigan, Ann Arbor, MI USA

**Spacecraft magnetic field measurements are frequently degraded by stray magnetic fields originating from onboard electrical systems. These interference signals can mask the natural ambient magnetic field, reducing the quality of scientific data collected. Traditional approaches involve positioning magnetometers on mechanical booms to minimize the influence of the spacecraft's stray magnetic fields. However, this method is impractical for resource-constrained platforms, such as CubeSats, which necessitate compact and cost-effective designs. In this work, we introduce an interference removal technique called wavelet-adaptive interference cancellation for underdetermined platforms (WAIC-UP). This method effectively eliminates stray magnetic field signals using multiple magnetometers, without requiring prior knowledge of the spectral content, location, or magnitude of the interference signals. WAIC-UP capitalizes on the distinct spectral properties of various interference signals and employs an analytical method to separate them from ambient magnetic field in the wavelet domain. We validate the efficacy of WAIC-UP through a statistical simulation of randomized 1 U CubeSat interference configurations, as well as with real-world magnetic field signals generated by copper coils. Our findings demonstrate that WAIC-UP consistently retrieves the ambient magnetic field under various interference conditions and does so with orders of magnitude less computational time compared to other modern noise removal algorithms. By facilitating high-quality magnetic field measurements on boomless platforms, WAIC-UP presents new opportunities for small-satellite-based space science missions.**

Manuscript received 26 May 2023; revised 6 September 2023; accepted 11 September 2023. Date of publication 14 September 2023; date of current version 8 December 2023.

DOI. No. 10.1109/TAES.2023.3315220

Refereeing of this contribution was handled by H. Mir.

This work was supported by NASA Grant 80NSSC22M0104 and Grant 80GSFC20C0075.

Authors' addresses: Alex P. Hoffmann and Mark B. Moldwin are with the Department of Climate and Space Sciences and Engineering, College of Engineering, University of Michigan, Ann Arbor, MI 48109 USA, E-mail: (aphoff@umich.edu; mmoldwin@umich.edu). *(Corresponding author: Alex P. Hoffmann.)*



## I. INTRODUCTION

Magnetometers are used on spacecraft to measure the heliospheric magnetic field [1], Earth's magnetosphere [2], and other planetary magnetospheres [3]. However, spacecraft electrical systems can generate stray magnetic fields which interfere with the measurements of natural ambient magnetic field [4]. To minimize this interference, magnetometers are typically positioned at the end of a mechanical boom. For example, the future mission to Mars, escape and plasma acceleration and dynamics explorers (EscaPADE), consists of two SmallSats, each equipped with magnetometers on the end of a 90-cm boom [5]. However, satellite booms increase the cost and complexity of spacecraft designs, limiting their adoption for small as well as some large complex satellites. Consequently, numerous space exploration missions have forgone the inclusion of a magnetometer altogether (e.g., the NASA Dawn and New Horizons missions).

Various techniques have been developed to eliminate stray magnetic fields from spacecraft measurements using multiple magnetometers without a boom. Some of these techniques employ principal component analysis (PCA) [6] or independent component analysis (ICA) [7] to isolate stray magnetic field signals based on their statistical properties. However, these methods presuppose fewer noise sources than magnetometers or magnetometer axes. This is rarely the case since spacecraft typically have many electrical subsystems [8]. A more generalized approach, underdetermined blind source separation (UBSS), relies on cluster analysis and compressive sensing to separate signals based on their spectral composition [9], [10]. Although UBSS outperforms PCA and ICA, it is computationally demanding and necessitates that the interference and ambient magnetic field signals have sparse spectral signatures. This strict assumption of spectral sparsity may not be applicable to every spacecraft magnetic field environment. Another technique, multivariate singular spectrum analysis (MSSA), decomposes time series measurements using an eigenvalue decomposition without relying on assumptions about source signals [11]. However, selecting the appropriate components to reconstruct the ambient magnetic field proves challenging and is prone to user error.

In this work, we introduce a novel algorithm, wavelet-adaptive interference cancellation for underdetermined platforms (WAIC-UP), designed to remove stray magnetic fields from boomless spacecraft magnetometer measurements. Our algorithm leverages the statistical correlation between magnetometer signals' wavelet coefficients to identify interference signals. WAIC-UP expands upon

the method of Sheinker and Moldwin [12], which separates a single interference signal using two magnetometers. This method is ill-suited for boomless platforms with multiple interference sources that cannot be modeled as a single dipole field. However, by applying the method on a wavelet basis, WAIC-UP can accommodate multiple interference sources with distinct spectral characteristics. Furthermore, WAIC-UP can employ more than two magnetometers to enhance its performance and reliability. The WAIC-UP algorithm assumes that the ambient magnetic field is uniform across the magnetometers, the interference signals are uncorrelated with the ambient magnetic field, the interference signals have varying amplitudes at different magnetometers, and each wavelet scale contains fewer interference signals than magnetometers. In wavelet analysis, the scale refers to the relative width of a wavelet, and determines the specific frequency and time window under analysis.

We outline the analytical foundation of the WAIC-UP algorithm and describe three experimental procedures employed to validate its performance. The first two experiments utilize publicly available data from two mock CubeSat experiments to demonstrate the separation of real magnetic field data produced by current-driven copper coils from spacecraft magnetic field measurements [9]. The second experiment presents a statistical analysis of thousands of 1 U CubeSat simulations using randomized stray magnetic field signals and source locations. The implementation of the WAIC-UP algorithm enables high-quality magnetic field measurements on boomless platforms, ultimately reducing the cost and complexity of spacecraft design and paving the way for new opportunities in small-satellite-based space science missions.

## II. METHODOLOGY

### A. Linear Mixing Model for Magnetic Field Measurements

In this section, we consider a spacecraft equipped with multiple magnetometers that measure both the ambient magnetic field and time-varying stray magnetic fields. Since there are more interference sources than magnetometers, reconstructing the ambient magnetic field from these measurements is an underdetermined problem.

A common approach to simplify this problem is to place the magnetometers on a mechanical boom in a colinear arrangement, enabling multiple stray magnetic fields to be approximated as a single dipole field. This results in a linear mixing model given by

$$\begin{bmatrix} B_{\text{out}}(t,k) \\ B_{in}(t,k) \end{bmatrix} = \begin{bmatrix} 1 & 1 \\ 1 & k \end{bmatrix} \begin{bmatrix} S_1(t,k) \\ S_2(t,k) \end{bmatrix}. \tag{1}$$

Here, $S_1(t,k)$ represents the ambient magnetic field signal, $S_2(t,k)$ denotes the accumulated stray magnetic field signal, and $k$ is a gain factor that defines the magnitude difference between the inboard and outboard magnetometers.

However, this approach is not feasible for boomless platforms, where multiple interference sources cannot be modeled as a single dipole field. In this situation, we have a more general linear mixing model given by

$$\begin{bmatrix} B_1(t,k) \\ \vdots \\ B_m(t,k) \end{bmatrix} = \begin{bmatrix} 1 & k_{12} & \dots & k_{1n} \\ \vdots & \vdots & \ddots & \vdots \\ 1 & k_{m2} & \dots & k_{mn} \end{bmatrix} \begin{bmatrix} S_1(t,k) \\ \vdots \\ S_n(t,k) \end{bmatrix}. \tag{2}$$

In this equation, $m$ is the number of magnetometers and $n$ is the number of interference sources ($m < n$). This system has an infinite solution space, necessitating sophisticated demixing algorithms like compressive sensing.

The WAIC-UP algorithm exploits the statistical correlation between wavelet coefficients of magnetometer signals to separate the ambient magnetic field from interference signals. WAIC-UP extends the method in [12] which removes a single interference signal using two magnetometers. However, WAIC-UP can handle multiple interference sources with different spectral characteristics using two or more noncolinear magnetometers on a boomless platform. WAIC-UP achieves this by approximating the complex time-domain linear mixing system in (2) as the mixing system in (1) in the time-scale domain.

### B. Wavelet-Based Interference Estimation for Two Magnetometers

In this section, we introduce an extension of an adaptive interference removal technique for estimating and removing stray magnetic field signals from mixed magnetometer measurements using a wavelet-transform. We consider a spacecraft with two magnetometers mounted on its bus, exposed to multiple stray magnetic field signals from onboard electrical systems. The magnitude and frequency of these signals vary according to the spacecraft's configuration and operation mode. We do not assume any prior knowledge of the interference source locations or spectral contents, except that the interference signal is uncorrelated with the ambient magnetic field signal.

The mixed magnetometer signals in the discrete-time domain, denoted as $b_1(n)$ and $b_2(n)$, contain both the ambient magnetic field signal and the stray magnetic field signals. The first step of the WAIC-UP algorithm is to detrend the data using a uniform filter. WAIC-UP is sensitive to low-frequency interference whose time-frequency estimation is invalid due to the shrinking cone of influence at low frequencies. After detrending the data, we apply the wavelet-transform to these signals using a Morlet wavelet function $\psi(\eta) = \pi^{-1/4} e^{i\omega_0 \eta} e^{-\eta^2/2}$, where $\omega_0$ is a nondimensional frequency variable and $\eta$ is a nondimensional time parameter. The wavelet-transform is defined as

$$W(s) = \sum_{n'=0}^{N-1} b\left(n'\right) \psi^* \left( \frac{n'-n}{s} \right) dt. \tag{3}$$

The scale parameter $s$ determines the frequency resolution, and the translation parameter $n'$ determines the time resolution of the wavelet-transform. The complex conjugate of $\psi$ is denoted by $\psi^*$. The wavelet-transform generates a

series of coefficients, $W(s)$, that reveal the time-frequency spectrum of the magnetometer signals, $b(n)$.

We represent the wavelet series of $b_1(n)$ and $b_2(n)$ as $W_1(s)$ and $W_2(s)$. For each scale $s$, these series can be expressed as

$$\begin{cases} W_1(s) = X(s) + A(s) + \omega_1(s) \\ W_2(s) = X(s) + KA(s) + \omega_2(s). \end{cases} \tag{4}$$

In these equations, $X(s)$ represents the wavelet series of the ambient magnetic field signal we aim to recover, $A(s)$ denotes the wavelet series of the stray magnetic field signals at each scale, $K$ is the gain factor indicating the influence of the interference signal at each magnetometer, and $\omega_1(s)$ and $\omega_2(s)$ are random normal noise terms accounting for measurement errors.

Our objective is to estimate the ambient magnetic field $X(s)$ by identifying and eliminating $A(s)$. To accomplish this, we must estimate two unknown parameters: $K$ and $A(s)$. The algorithm's first step is to estimate the gain $K$ for each wavelet scale. Following that, we estimate the stray magnetic field signal at each scale and subtract the estimated interference signal from the mixed magnetometer signals to reconstruct the wavelet coefficients of the ambient magnetic field signal.

To estimate the gain $K$ at each wavelet scale, we compute the difference between the noisy magnetometer measurements $W_1(s)$ and $W_2(s)$, thereby eliminating $X(s)$ from (4)

$$\begin{cases} D(s) = W_2(s) - W_1(s) \\ D(s) = (K-1)A(s) + \omega_2(s) - \omega_1(s). \end{cases} \tag{5}$$

Assuming that the interference signals and ambient magnetic field signal are uncorrelated, calculating the correlation of the signal difference $D(s)$ with the noisy magnetometer data $W_1(s)$ and $W_2(s)$ yields

$$\begin{cases} C_1 = \sum D(s)W_1(s) \\ C_1 = (K-1)\sum A^2(s) - \sum \omega_1^2(s) \end{cases} \tag{6}$$

$$\begin{cases} C_2 = \sum D(s)W_2(s) \\ C_2 = K(K-1)\sum A^2(s) + \sum \omega_2^2(s). \end{cases} \tag{7}$$

Note that while the correlation term $C_1$ has a factor of $K$-1, the correlation term $C_2$ has a factor of $K(K$-1). Dividing $C_2$ by $C_1$ provides an estimation $\hat{K}$ of the gain $K$

$$\hat{K} = \frac{C_2}{C_1} = \frac{K(K-1)\sum A^2(s) + \sum \omega_2^2(s)}{(K-1)\sum A^2(s) - \sum \omega_1^2(s)}. \tag{8}$$

If the power of the stray magnetic field signal $\sum A^2(s)$ is significantly larger than the random normal noise signals, $\sum \omega_1^2(s)$ and $\sum \omega_2^2(s)$, then the estimator $\hat{K}$ will converge to K.

Using the estimated gain $\hat{K}$ we can calculate the interference signal $A(s)$ with the following equation:

$$A(s) = \frac{W_2(s) - W_1(s)}{\hat{K} - 1}. \tag{9}$$

With the stray magnetic field signal estimate, we can subtract it from the magnetometer signals to obtain the wavelet coefficients of the ambient magnetic field, as follows:

$$X(s) = \frac{\hat{K}W_1(s) - W_2(s)}{\hat{K} - 1}. \tag{10}$$

Having removed the stray magnetic field interference from the mixed magnetometer measurements, we can now reconstruct the time series signal of the ambient magnetic field utilizing [13]

$$b(n) = \frac{\delta j \delta t^{1/2}}{C_\delta \Psi_0(0)} \sum_{j=1}^{J} \frac{\mathbb{R}\left\{X\left(s_j\right)\right\}}{s_j^{1/2}}. \tag{11}$$

In this equation, $C_\delta$ represents a scale-independent constant dependent on the wavelet function. The term $\Psi_0(0)$ corresponds to the value of the wavelet function at zero, which, for a Morlet wavelet function, is $\pi^{-1/4}$. For a Morlet wavelet function, $C_\delta$ is approximately 0.776. The term $\delta j$ denotes the spacing between discrete scales, and $dt$ refers to the sampling period of the time series. Lastly, $Re(X(s_j))$ is the real part of the wavelet coefficients of the ambient magnetic field signal.

### C. Generalizing WAIC-UP for Multiple Magnetometers

In situations where stray magnetic field signals are present at mutually exclusive wavelet scales, the mixing system of the interference and ambient magnetic field signals can be described by (1). In such cases, the WAIC-UP algorithm is capable of identifying and removing stray magnetic field interference. However, if multiple different interference signals exist within the same wavelet-scale, the mixing system is defined by (2). The adaptive interference removal algorithm described earlier would be unable to estimate the gains for each interference signal in this scenario. Nevertheless, for spacecraft equipped with more than two magnetometers, it is possible to find the pairwise combination of magnetometers with the least interference.

We apply the algorithm from Section II-B (denoted as the function *clean()*) to each pair of magnetometers. The magnetometer signals are represented as $B(n) = [b_1(n), b_2(n) \ldots b_m(n)]$, and their wavelet series as $W(s) = [W_1(s), W_2(s) \ldots W_m(s)]$, obtained using (3). We estimate a series of ambient magnetic field signals $X(s) = [X_1(s), X_2(s) \ldots X_Z(s)]$, where $Z = \frac{M(M-1)}{2}$ is the number of unique pairs. We define a new ambient magnetic field signal $X_f(s)$ by selecting the minimum magnitude among $X(s)$ for each scale and time point. The algorithm is summarized as follows.

Owing to the spatial structure of magnetic fields (i.e., dipolar, quadrupolar, etc.), it is highly likely that some stray magnetic fields may not appear at all on the axis of one magnetometer while having a large magnitude at another magnetometer. As a result of this spatial structure, the performance of the WAIC-UP algorithm improves with each additional spatially distributed magnetometer.

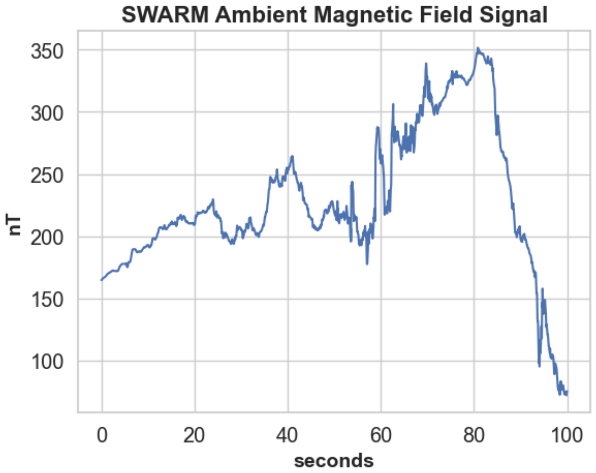


Fig. 1. Magnetic perturbation signal generated by subtracting the IGRF magnetic field model from in situ observations by the SWARM A satellite on March 17th, 2015 between 8:53 and 8:55 UTC.

**Algorithm 1:** WAIC-UP for Multiple Magnetometers.

**Input**: B(n)
**Output**: x(n)
*Initialization*:
W(s) $= \Psi\{B(n)\}$
Pairs $= (i, j) \mid i \in \text{range}(m)$ and $j \in \text{range}(i+1, m)$ *Clean All Pairwise Combinations*
**for** $(i, j) \in$ *Pairs* **do**
  $X(s) \leftarrow X(s) + [clean(W_i(s), W_j(s))]$
**end for**
*Save Time-Scale Points with Minimum Interference*
**for** $(\tau, s_j) \in (\tau \in T, j = 1, \ldots, J)$ **do**
  $i = argmin(|X(s_j, \tau)|)$
  $X_f(s_j, \tau) \leftarrow X_i(s_j, \tau)$
**end for**
x(n) $= \Psi^{-1}\{X_f(s)\}$
**return** x(n)

## III. EXPERIMENTAL EVALUATION OF WAIC-UP WITH REAL AND SIMULATED DATA

We evaluated the WAIC-UP algorithm on three experiments involving boomless platforms. The first two experiments utilized a mock CubeSat [14] platform with laboratory-generated interference signals from an open-source dataset [9]. The third experiment simulated a CubeSat with random interference signals and source locations. In every experiment, we used geomagnetic perturbation data from the SWARM A spacecraft as the ambient magnetic field signal. The SWARM A spacecraft recorded this data on March 17th, 2015 between 8:53 and 8:55 UTC, while flying over the southern auroral zone between the 69th and 76th parallel south. This segment of the orbit contains a higher concentration of high-frequency signal content and is depicted in Fig. 1.

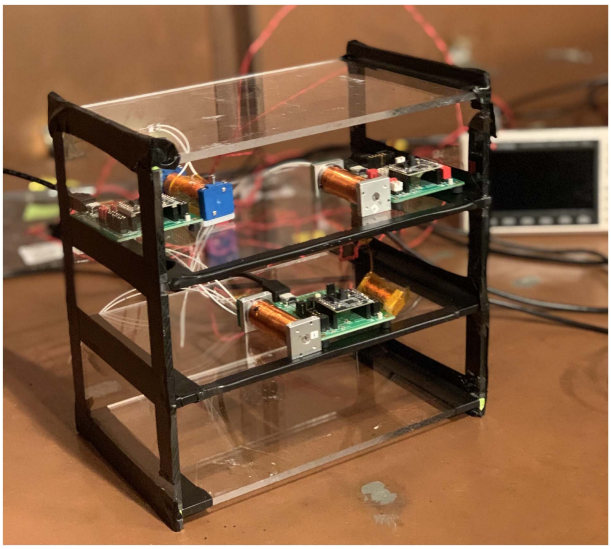

Fig. 2. Experimental setup with the mock CubeSat apparatus, three PNI RM3100 magnetometers, and four copper coils driven by signal generators. The mock CubeSat is placed within a copper room to act as a shield can, blocking stray magnetic fields from the surrounding environment that are not part of the experiment.

### A. WAIC-UP Application to Real Magnetic Field Data

We conducted two experiments to assess the WAIC-UP algorithm using real-world data. Both experiments employed real stray magnetic field data from open-source datasets. These datasets utilized current-driven copper coils inside a mock CubeSat to generate stray magnetic field signals. We measured these signals using PNI RM3100 magnetometers in a copper room shielded by mu-metal. The copper room acts as a shield can to isolate the experiment from external magnetic fields, and was designed and characterized to have an attenuation factor of 37 dB at 105 Hz. The experimental mock CubeSat setup is shown in Fig. 2.

The PNI RM3100 is a low-cost magneto-inductive magnetometer that exhibits increased measurement uncertainty at higher sampling rates [15]. The first dataset featured three PNI RM3100 magnetometers and four copper coils, which generated a 0.8-Hz sine wave, a 0.4-Hz sine wave, a 1-Hz square wave, and a 2-Hz square wave. The magnetometers were sampled for a total of 100 s at 50 Hz ($N = 5000$) and have an expected measurement uncertainty of 8 nT. We virtually added the SWARM magnetic perturbation data to each magnetometer to simulate the ambient magnetic field. Fig. 3 displays the initial 20 s of the mixed magnetometer signals.

We applied the WAIC-UP algorithm to the three magnetometer measurements to derive the estimated ambient magnetic field signal. The low-frequency trend was removed by subtracting the signal applied with a uniform filter of $n = 500$. The mean trend was added back after applying the WAIC-UP algorithm. We compared the results with those obtained using a single magnetometer with the least interference present (denoted *minimum*), and UBSS. To evaluate performance, we employed four metrics: 1) signal-to-noise

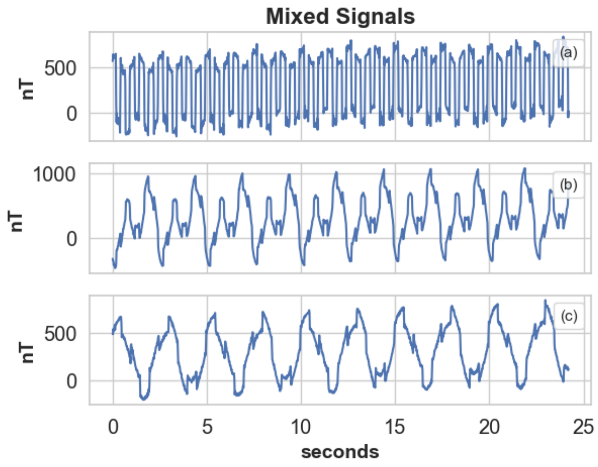


Fig. 3. Plots (a), (b), and (c) depict 20 s of mixed stray magnetic field data recorded by three PNI RM3100 magnetometers.

TABLE I
Summary of Three Magnetometer Results

| | $\rho$ | SNR (dB) | RMSE (nT) | Time (s) |
|---|---|---|---|---|
| Minimum | 0.6843 | -0.649 | 259.68 | – |
| UBSS | 0.9993 | 28.75 | 8.79 | 44.35 |
| **WAIC-UP** | 0.9993 | 28.48 | 9.08 | 1.78 |

ratio (SNR), 2) Pearson correlation coefficient ($\rho$), 3) root mean square error (RMSE), and 4) execution run-time.

The SNR is calculated as follows, where $x_i$ represents the true signal value, $\bar{x}$ is the mean of the true signal, $y_i$ is the estimated signal value, and $n$ is the number of data points

$$\text{SNR (dB)} = 10\log_{10}\frac{\sum_{i=1}^{n}(x_i-\bar{x})^2}{\sum_{i=1}^{n}(x_i-y_i)^2}. \tag{12}$$

The Pearson correlation coefficient is calculated using (13), where $x_i$ and $y_i$ are the true and estimated signal values, respectively, $\bar{x}$ and $\bar{y}$ are the means of the true and estimated signals, respectively, and $n$ is the number of data points

$$\rho = \frac{\sum_{i=1}^{n}(x_i-\bar{x})(y_i-\bar{y})}{\sqrt{\sum_{i=1}^{n}(x_i-\bar{x})^2}\sqrt{\sum_{i=1}^{n}(y_i-\bar{y})^2}}. \tag{13}$$

The RMSE is calculated using (14), where $x_i$ and $y_i$ are the true and estimated signal values, and $n$ is the number of data points

$$\text{RMSE (nT)} = \sqrt{\frac{\sum_{i=1}^{n}(x_i-y_i)^2}{n}}. \tag{14}$$

Table I summarizes the results of the first experiment, which involved three magnetometers and four noise sources. The execution time for each algorithm, using an Intel Core i7-1255 U CPU, is presented in the Time column. The UBSS algorithm is parallelizable and hence was executed using ten processes, while the WAIC-UP algorithm utilized a single process.

For the second experiment, the dataset was generated using four copper coils and a Quad-Mag. The Quad-Mag is an experimental CubeSat magnetometer that consists of four PNI RM3100 magnetometers on an integrated electronics board [16]. The Quad-Mag was positioned at the bottom of the mock CubeSat. Four copper coils were placed above the mock CubeSat within the 3 U CubeSat volume. The copper coils were driven by a 0.8-Hz sine wave, a 5-Hz sine wave, a 2-Hz sawtooth wave, and a 3-Hz attenuating sine wave. The signals were sampled for a total of 150 s at 65 Hz ($N = 9750$). At this frequency, a single PNI RM3100 magnetometer has a measurement uncertainty of approximately 10.5 nT. We virtually added the SWARM magnetic perturbation data to each magnetometer in the Quad-Mag to simulate the ambient magnetic field.

TABLE II
Summary of Quad-Mag Results

| | $\rho$ | SNR (dB) | RMSE (nT) | Time (s) |
|---|---|---|---|---|
| Minimum | 0.8075 | 2.76 | 42.33 | – |
| UBSS | 0.9971 | 22.33 | 4.40 | 102.78 |
| **WAIC-UP** | 0.9964 | 21.42 | 4.94 | 4.61 |

The results of applying WAIC-UP to separate the interference signals from the ambient magnetic field signal are shown in Table II.

These results demonstrate that WAIC-UP achieved comparable correlation, SNR, and RMSE to UBSS, but with significantly less execution time. The reduced computational complexity of the WAIC-UP algorithm allows us to test the effectiveness of WAIC-UP using more data-intensive methods. In Section III-B, we present a Monte Carlo simulation of WAIC-UP applied to stray magnetic field noise present in a 1 U CubeSat.

### B. Simulation of Randomized Interference Sources

We evaluated the performance of the WAIC-UP algorithm by conducting thousands of simulations with randomized noise source locations and stray magnetic field signals. The Magpylib Library was used to simulate the stray magnetic field signals [17]. We simulated four magnetic dipoles as interference sources and four virtual magnetometers in the Quad-Mag configuration. The dipoles were placed randomly within a 1 U ($10 \times 10 \times 10$ cm) volume and at least 10 mm above the virtual Quad-Mag. The dipole noise sources were modeled with current loops that have magnetic moments between $1.57 \times 10^{-4}\text{Am}^2$ and $5.89 \times 10^{-4}\text{Am}^2$ (i.e., up to 500 nT at 5 cm). To simulate a worst-case scenario, the dipoles were aligned such that their noise signals cumulatively added to each other. It is important to note that Magpylib's simulation of stray magnetic field interference does not account for the presence of conductors or induction currents that may be present in a spacecraft. Fig. 4 illustrates a virtual CubeSat with four interference sources and four sensors.

In each simulation, we collected 100 s of data from the virtual magnetometers sampled at 50 Hz. We added 10 nT of random normal noise to mimic the measurement uncertainty

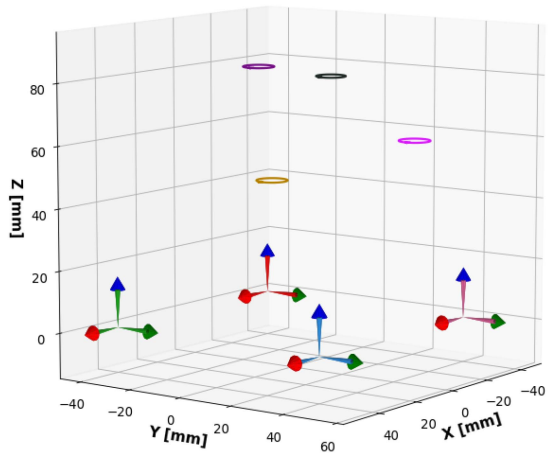


Fig. 4. 1 U CubeSat with four dipole interference sources (rings) and four virtual magnetometers (tricolor vectors). The interference sources have different positions in millimeters: (−33, 22, 18), (−18, −35, 73), (47, 7, 70), and (33, −2, 36).

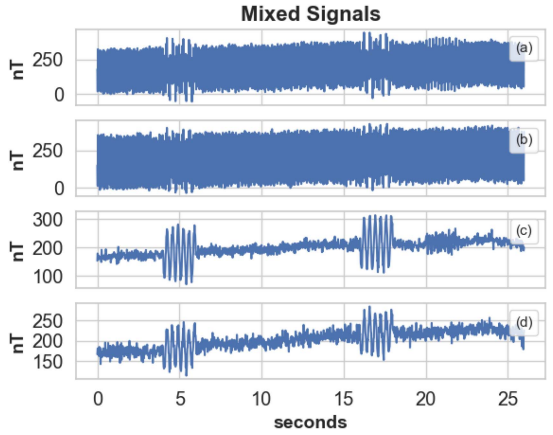


Fig. 5. 26 s of mixed magnetometer data. The virtual magnetometers are in a Quad-Mag configuration and sampled the signals at 50 Hz with 10 nT of random normal noise added.

of a PNI RM3100 magnetometer at this sample rate. To simulate the stray magnetic field signals, we generated three source signals. These source signals include a simulated reaction wheel signal with 15- and 20-Hz components, a square wave with a principal frequency of 5 Hz, and a 3-Hz sine wave. The sine and square wave source signals were randomly turned ON and OFFthroughout the window. The fourth stray magnetic field was a 24-h sample of interference taken from the Michibiki-1 magnetometers. The interference was calculated using the simple formula $b_{\text{interference}} = b_{in} - b_{\text{out}}$, in order to subtract the ambient magnetic field. This is a 1-Hz signal that was randomized by selecting a random slice with the same length as the 100-s, 50-Hz signal. The same SWARM A magnetic perturbation data were added equally to each virtual magnetometer in every simulation. Fig. 5 shows a 26-s plot of the noisy magnetometer signals from the simulation with the same source configuration, as in Fig. 4. The four interference signals are clearly visible as periodic fluctuations on top of the ambient signal. The interference signals have different

TABLE III
Median Results of Randomized Stray Magnetic Field Simulations

| | $\rho$ | SNR (dB) | RMSE (nT) |
|---|---|---|---|
| Average | 0.6295 | -2.42 | 76.88 |
| Minimum | 0.2468 | -12.39 | 26.31 |
| **WAICUP** | 0.9937 | 14.21 | 11.33 |

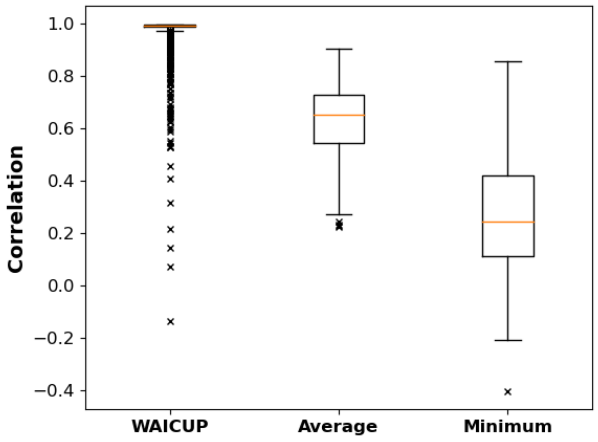


Fig. 6. This plot shows the boxplots of the correlation of the the true ambient magnetic field signal with the minimum, averaged signal, and WAIC-UP signals.

frequencies and amplitudes, and they affect each magnetometer differently.

We conducted 1550 randomized simulations and recorded the RMSE, correlation, and SNR for the magnetometer with the least interference in each simulation (denoted *minimum*), the four-magnetometer averaged signal, and the signal cleaned by WAIC-UP. In each simulation, the low-frequency trend was removed by subtracting the signal applied with a uniform filter of $n = 500$. The mean trend was added back after applying the WAIC-UP algorithm. Table III presents the median results of the 1550 randomized simulations. WAIC-UP outperformed both the minimum and the averaged signals, achieving higher correlation and SNR, as well as lower RMSE. However, the median RMSE of WAIC-UP is larger than the lower bound average normal error of 5 nT for the Quad-Mag.

We compared the correlation of the WAIC-UP, minimum, and averaged signals to the true ambient magnetic field signal. Fig. 6 displays the box plots of the correlation coefficients for the randomized simulations. The box plots demonstrate that WAIC-UP can enhance the median correlation to above 0.99, with only a few outliers below 0.98. The averaged signal exhibits a higher correlation than the minimum magnetometer signal, but both have significantly lower correlations compared to the WAIC-UP signal.

In addition, we compared the RMSE of the minimum, averaged, and cleaned signals to the true ambient magnetic field signal. Fig. 7 presents the box plots of the log RMSE for the simulations. The box plots reveal that WAIC-UP

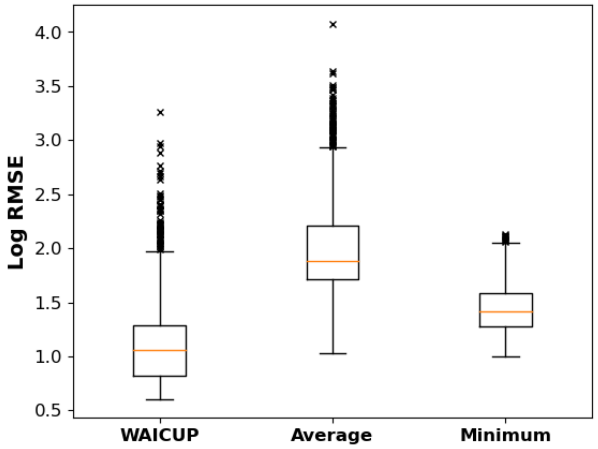


Fig. 7. This plot shows the boxplots of the log-transformed root mean square error (RMSE) values for the raw magnetometer signal from a single magnetometer, the averaged signal, and the signal cleaned with WAIC-UP. The RMSE values are measured in nanoTesla (nT).

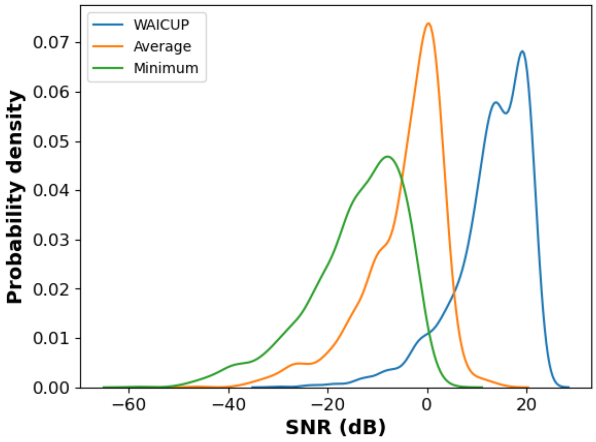


Fig. 9. Probability distribution function of the SNR values for the minimum, averaged, and WAIC-UP signals over the 1550 randomized simulations.

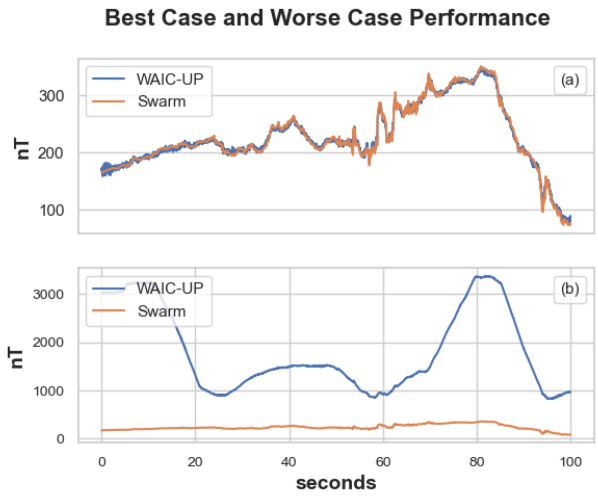


Fig. 8. Top panel (a) shows the best case scenario where the RMSE of the WAIC-UP signal is 4.025 nT. The WAIC-UP signal is shown in blue and the true Swarm signal is shown in orange. The discrepancy is due to the lack of random normal noise in the orange signal. The bottom panel (b) shows the worst-case scenario where WAIC-UP cleans the signal, but there is large amplitude noise in a frequency that is below the band WAIC-UP is applied to.

can significantly reduce the RMSE by several orders of magnitude. The lowest RMSE achieved by WAIC-UP was 4.03 nT, down from an average of 66.71 nT. The highest RMSE achieved by WAIC-UP was 1802.72 nT, reduced from an average of 1890.75 nT. In this simulation with high interference, three of the interference sources were placed very close to each other and directly above one virtual magnetometer, and the noise source corresponding to the Michibiki-1 signal has a low-frequency, large-magnitude trend that is removed before applying WAIC-UP and added after to retrend the data.

To provide a visual example of WAIC-UP's performance, Fig. 8 shows time series plots for the best case and worst case scenarios. The top panel (a) illustrates a case where WAIC-UP effectively removes the interference, reducing the RMSE from 66.71 to 4.025 nT. The cleaned signal closely tracks the true signal. The bottom panel (b) shows a challenging case where large amplitude, low-frequency interference remains after WAIC-UP, leading to an RMSE of 1802.72 nT improved from 1890.75 nT. This case is the largest outlier in Fig. 7, and the significant error is due to the fact that one of the noise sources is very close to a magnetometer and is composed of low-frequency noise that is hidden from WAIC-UP due to the detrending process. These examples demonstrate WAIC-UP's capabilities and limitations. WAIC-UP excels at removing interference within its filtering bands but struggles with low-frequency noise due to the cone of influence in wavelet analysis. However, this can be addressed by using a window size larger that 100 s to expand the cone of influence.

We evaluated the SNR of the minimum, WAIC-UP, and averaged magnetometer signals. Fig. 9 illustrates the probability distribution of the SNR values. Both the averaged and minimum signals have a mean SNR below 0 dB. The distribution of the WAIC-UP SNR is shifted to the right of the average and minimum signals, signifying a substantial improvement in SNR. Interestingly, the WAIC-UP SNR distribution has a bimodal peak at 19.1 and 13.9 dB. When comparing the change in SNR among the three signals, WAIC-UP had a mean increase of $\Delta$17.5 dB from the averaged signal and $\Delta$27.06 dB from the minimum signal. This indicates that the use of WAIC-UP can significantly enhance the SNR of the magnetometer signal compared to simply averaging or using the magnetometer with the least interference. We also observe from this distribution that 92.6% of the SNR values for WAIC-UP are above 0 dB while the minimum magnetometer signal has 0.9% of the SNR values above 0 dB.

Lastly, we assess the distribution of the correlation and SNR of the WAIC-UP signals. Fig. 10 displays a scatter plot of the correlation and SNR of the WAIC-UP signals from the randomized simulations. The data points are colored by density, with subplots at the top and to the right depicting the distribution of data points along each axis. This plot

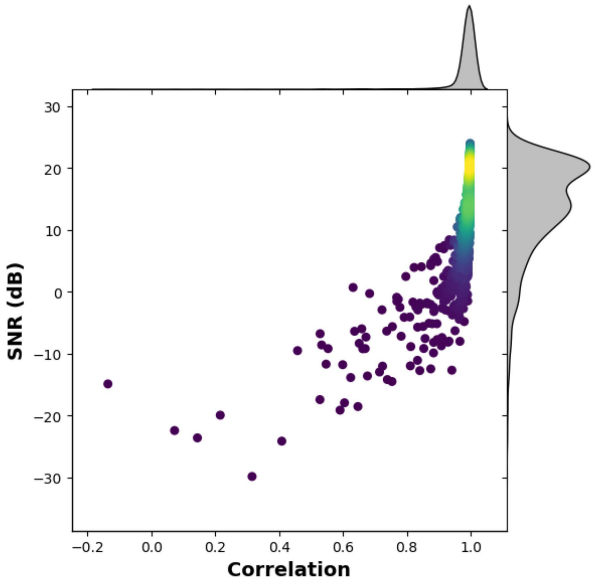


Fig. 10. Figure shows the distribution of the correlation and SNR of the WAIC-UP signals. The top panel displays the probability distribution of the correlation, while the right panel exhibits the probability distribution of the SNR.

demonstrates that WAIC-UP is highly effective at increasing the correlation to nearly 1.

The simulation results demonstrate that WAIC-UP is an effective method for cleaning magnetometer signals in the presence of stray magnetic field interference. This approach not only reduces the RMSE and significantly enhances the SNR but also improves the correlation coefficient between the estimated and true signals. The results also indicate that WAIC-UP performs far better than simply taking the magnetometer with the least noise present or averaging the magnetometer signals.

## IV. DISCUSSION

In the experiments conducted using real magnetic field data from open-source datasets, we observed that WAIC-UP effectively removed stray magnetic field interference from magnetometer measurements in a boomless configuration. The first dataset involved three PNI RM3100 magnetometers and four stray magnetic field signals, while the second dataset used the Quad-Mag magnetometer and four stray magnetic field signals. In the first experiment, the magnetometer with the least interference had an RMSE of 260 nT. WAIC-UP reduced this to 9.08 nT, and UBSS reduced the interference to 8.79 nT. Both algorithms improved the SNR by over 28 dB and increased the correlation to above 0.999. In the second experiment with the Quad-Mag, the magnetometer with the least interference had an RMSE of 42.33 nT. WAIC-UP and UBSS managed to reduce the interference to 4.94 and 4.40 nT, respectively. This result was below the expected measurement uncertainty for sampling the PNI RM3100 at 65 Hz. WAIC-UP also achieved comparable results to UBSS in terms of correlation and SNR. The magnetometer settings in these experiments had different random normal noise characteristics and sample rates. The spectral content of the stray magnetic field interference varied as well. Despite these differences, WAIC-UP consistently achieved comparable results in both experiments. The significant difference between WAIC-UP and UBSS is that WAIC-UP has a lower computational complexity, with over a factor of 20 reduction in run-time from 102.78 s by UBSS to 4.61 s by WAIC-UP when processing nearly 10 000 data points in the second experiment.

Subsequently, we conducted over 1500 randomized simulations to perform a statistical analysis of WAIC-UP's efficacy. In these simulations, stray magnetic field interference sources were randomly located and turned ON and OFF sporadically. Real spacecraft interference data from the Michibiki-1 satellite were also incorporated as an interference signal. WAIC-UP consistently achieved a correlation with the true magnetic field exceeding 0.99 in these simulations. The median RMSE obtained from averaging the Quad-Mag signals was nearly 77 nT, while the median RMSE from the WAIC-UP signals was 11.33 nT. Our simulations added 10 nT of random normal error to each virtual magnetometer in order to match the specifications of the PNI RM3100 magnetometer, but most heliophysics research demands magnetic field measurements with accuracy better than 1 nT. Despite this, the 11.33-nT RMSE is suitable for attitude determination and many magnetospheric science investigations, such as monitoring field-aligned currents.

The WAIC-UP algorithm operates under certain assumptions that may limit its applicability. First, it assumes that the ambient magnetic field signals and the interference signals have no correlation. Second, it assumes that the interference signals occupy distinct wavelet scales. In addition, WAIC-UP assumes that the interference signal is much larger than the random normal noise of the magnetometer. If these assumptions are violated, the algorithm might produce inaccurate results. However, a possible solution to multiple interference signals occupying the same scale-band is to use more than two magnetometers and find the optimal pair of magnetometers with the minimum interference level. We found that adding more spatially distributed magnetometers improves the performance of the algorithm. Quantitatively characterizing the performance of WAIC-UP with respect to the number of magnetometers is a potential area of future work. It is worth noting that WAIC-UP is a blind algorithm, but in real satellite scenarios, we often know the noise sources' locations and potentially their spectral signatures. These simulations could inform future magnetic cleanliness designs. Future research could also explore alternative wavelet transforms that offer better time-frequency resolution than the Morlet wavelet used in this study. Another challenge posed by this algorithm is its inability to handle low-frequency signals, which are crucial for space physics research. Space physics research often relies on absolute magnetic field measurements to determine the behavior of space plasmas. WAIC-UP detrends the magnetometer signals with a uniform filter and is not able to remove dc interference. However, other algorithms are available that can calibrate the dc offsets of magnetic field measurements

in situ [18]. Lastly, this algorithm was tested offline using a single thread on an Intel Core i7-1255 U CPU, which has much higher computational power than a typical CubeSat platform. A possible solution is to redesign the components of WAIC-UP (wavelet transform, correlation, median filter, etc.) into streaming signal operations, so that the algorithm can run in real-time onboard a CubeSat for operational purposes. This could be implemented on an FPGA or DSP microcontroller.

In this work, we developed a method for removing stray magnetic field interference from boomless spacecraft magnetometers. The WAIC-UP algorithm is an extension of an adaptive interference cancellation algorithm that can remove a single interference signal. WAIC-UP can remove interference in an underdetermined time-domain mixing system through taking a wavelet transformation. WAIC-UP performs similarly to UBSS, a leading interference removal algorithm. WAIC-UP also shows a very high correlation with the true magnetic field signal in many simulations. The WAIC-UP algorithm makes minimal assumptions about the stray magnetic field signals. The Monte Carlo simulations demonstrate that the algorithm can be applied to CubeSats with various interference sources, enabling low-cost boomless spacecraft for future space exploration.

## V. CONCLUSION

This article investigated the effectiveness of the WAIC-UP algorithm, a new wavelet-based noise identification method, in removing stray magnetic field interference from boomless spacecraft magnetometer measurements. Our findings demonstrated that the WAIC-UP algorithm offers performance comparable to the state-of-the-art UBSS interference removal algorithm, with a 20-fold reduction in execution time. In an experiment with three magnetometers and four interference signals, WAIC-UP achieved an increase in correlation from 0.6843 to 0.9993, an SNR improvement from −0.65 to 28.48 dB, and an RMSE reduction from 259.68 to 9.08 nT (near the normal noise floor of the instrument). Similarly, in an experiment with the Quad-Mag magnetometer and four interference signals, WAIC-UP yielded a correlation increase from 0.8075 to 0.9964, an SNR enhancement from 2.76 to 21.42 dB, and an RMSE reduction from 42.33 to 4.94 nT. These results highlight the significant improvements in magnetometer signal quality, which are crucial for various applications, including spacecraft navigation, attitude control, and space physics research.

In addition to conducting real-world experiments, we carried out over 1500 randomized simulations to statistically evaluate the efficacy of the WAIC-UP algorithm. The results revealed that WAIC-UP provides a substantially better estimation than merely selecting the magnetometer signal with the minimum noise. The median correlation increased from 0.2468 to 0.9937, the median SNR improvement was from −12.39 to 14.21 dB, and the median RMSE reduction was from 26.31 to 11.33 nT. Furthermore, the performance of the WAIC-UP cleaned signal significantly outperformed the results obtained by simply averaging the magnetometer signals. When comparing the WAIC-UP signals to the averaged magnetometer signals on a simulation-by-simulation basis, WAIC-UP demonstrated a mean increase in SNR of $\Delta$18.13 dB.

While the algorithm operates under certain assumptions that may limit its applicability, potential solutions and future research could address these limitations. Ultimately, WAIC-UP showcases its potential for application in CubeSats with diverse interference environments, facilitating the development of low-cost boomless spacecraft for future space exploration. The success of WAIC-UP in these experiments underscores its potential to facilitate more compact satellite designs, and represents a crucial step toward more efficient and cost-effective magnetometer designs for space missions.

## REFERENCES


[1] S. D. Bale et al., "The FIELDS instrument suite for solar probe plus," *Space Sci. Rev.*, vol. 204, no. 1, pp. 49–82, Dec. 2016.

[2] C. T. Russell et al., "The magnetospheric multiscale magnetometers," *Space Sci. Rev.*, vol. 199, no. 1, pp. 189–256, Mar. 2016.

[3] D. Banfield et al., "InSight auxiliary payload sensor suite (APSS)," *Space Sci. Rev.*, vol. 215, no. 1, Dec. 2018, Art. no. 4.

[4] M. Ludlam et al., "The THEMIS magnetic cleanliness program," *Space Sci. Rev.*, vol. 1, no. 141, pp. 171–184, Dec. 2008.

[5] R. J. Lillis et al., "Escapade: Coordinated multi-point observations of Ion and sputtered escape from Mars," in *Proc. 51st Annu. Lunar Planet. Sci. Conf.*, 2020, Art. no. 2470.

[6] O. D. Constantinescu, H.-U. Auster, M. Delva, O. Hillenmaier, W. Magnes, and F. Plaschke, "Maximum-variance gradiometer technique for removal of spacecraft-generated disturbances from magnetic field data," *Geoscientific Instrum., Methods Data Syst.*, vol. 9, no. 2, pp. 451–469, Dec. 2020.

[7] S. Imajo et al., "Signal and noise separation from satellite magnetic field data through independent component analysis: Prospect of magnetic measurements without boom and noise source information," *J. Geophysical Res.: Space Phys.*, vol. 126, no. 5, 2021, Art. no. e2020JA028790.

[8] S. A. Pope et al., "Exploring planetary magnetic environments using magnetically unclean spacecraft: A systems approach to VEX MAG data analysis," *Annales Geophysicae*, vol. 29, no. 4, pp. 639–647, 2011.

[9] A. P. Hoffmann and M. B. Moldwin, "Separation of spacecraft noise from geomagnetic field observations through density-based cluster analysis and compressive sensing," *J. Geophysical Res.: Space Phys.*, vol. 127, no. 9, 2022, Art. no. e2022JA030757.

[10] A. P. Hoffmann, M. B. Moldwin, B. P. Strabel, and L. V. Ojeda, "Enabling boomless CubeSat magnetic field measurements with the quad-mag magnetometer and an improved underdetermined blind source separation algorithm," *J. Geophysical Res.: Space Phys.*, vol. 128, 2023, Art. no. e2023JA031662.

[11] M. G. Finley, R. M. Broadfoot, S. Shekhar, and D. M. Miles, "Identification and removal of reaction wheel interference from in-situ magnetic field data using multichannel singular spectrum analysis," *J. Geophysical Res.: Space Phys.*, vol. 128, no. 2, 2023, doi: 10.1029/2022JA031020.

[12] A. Sheinker and M. B. Moldwin, "Adaptive interference cancelation using a pair of magnetometers," *IEEE Trans. Aerosp. Electron. Syst.*, vol. 52, no. 1, pp. 307–318, Feb. 2016.

[13] C. Torrence and G. P. Compo, "A practical guide to wavelet analysis," *Bull. Amer. Meteorological Soc.*, vol. 79, no. 1, pp. 61–78, Jan. 1998.

[14] A. A. Deshmukh, S. Sharma, J. W. Cutler, M. Moldwin, and C. Scott, "Simple regret minimization for contextual bandits," 2020, *arXiv:1810.07371*.

[15] L. H. Regoli et al., "Investigation of a low-cost magneto-inductive magnetometer for space science applications," *Geoscientific Instrum., Methods Data Syst.*, vol. 7, no. 1, pp. 129–142, Mar. 2018.
[16] B. P. Strabel et al., "Quad-Mag board for CubeSat applications," *Geoscientific Instrum., Methods Data Syst.*, vol. 11, no. 2, pp. 375–388, Nov. 2022.
[17] M. Ortner and L. G. C. Bandeira, "Magpylib: A free Python package for magnetic field computation," *SoftwareX*, vol. 11, Jan. 2020, Art. no. 100466, doi: 10.1016/j.softx.2020.100466.
[18] R. M. Broadfoot, D. M. Miles, W. Holley, and A. D. Howarth, "In situ calibration of the Swarm-Echo magnetometers," *Geoscientific Instrum., Methods Data Syst.*, vol. 11, no. 2, pp. 323–333, 2022.

**Alex P. Hoffmann** received the B.S.E. degree in computer science and engineering with a mathematics minor from the University of Iowa, Iowa City, IA, USA, in 2021. He is currently working toward the Ph.D. degree in climate and space sciences and engineering with the University of Michigan, Ann Arbor, MI, USA.

He is an Instrument Scientist for the magnetometers on the Geospace Dynamics Constellation and on the HERMES payload for the Lunar Gateway. His research interests include spaceborne magnetometers, signal processing, machine learning, and embedded systems.

Dr. Hoffman was the recipient of the University of Michigan Dean's Fellowship, the Michigan Institute for Plasma Science and Engineering Graduate Fellowship, and the NASA Future Investigators in NASA Earth and Space Science and Technology Fellowship.

**Mark B. Moldwin** received the B.A. degree in physics with honors from the University of Alaska-Fairbanks, Fairbanks, AK, USA, in 1987, and the M.A. and Ph.D. degrees in astronomy/space physics from Boston University, Boston, MA, USA, in 1990 and 1993, respectively.

He is currently an Arthur F. Thurnau Professor of Climate and Space Sciences and Engineering and Applied Physics with the University of Michigan (UM), Ann Arbor, MI, USA. He is also the Director of NASA's Michigan Space Grant Consortium and the Faculty Director of UM's M-STEM's M-Engin program. He has authored or coauthored two textbooks, over 200 articles and essays (including over 190 refereed scientific articles), and holds three patents on these subjects. His research interests include magnetospheric, ionospheric and heliospheric plasma physics, spaceborne magnetometers, signal processing, machine learning, and space science education and outreach.

Dr. Moldwin was the recipient of several awards, such as the AGU Waldo Smith Union Award in 2016, and the UM John F. Ulrich Educational Excellence Award in 2017. He is a Past-President of the AGU Education Section and a former Editor-in-Chief of *Reviews of Geophysics*.